DOI: 10.1002/chem.200600827

Studies of a Molecular Hourglass: Synthesis and Magnetic Characterisation of a Cyclic Dodecanuclear $\{Cr_{10}Cu_2\}$ Complex

Muralidharan Shanmugam,[a] Larry P. Engelhardt,[b] Finn K. Larsen,[c] Marshall Luban,*[b] Eric J. L. McInnes,[a] Christopher A. Muryn,[a] Jacob Overgaard,[c] Eva Rentschler,[d] Grigore A. Timco,[a] and Richard E. P. Winpenny*[a]

Abstract: The synthesis, structure, EPR, and magnetic studies of two dodecanuclear heterometallic cyclic clusters are reported. The compounds have the general formula $[R_2NH_2]_2[Cr_{10}Cu_2F_{14}(O_2CCMe_3)_{22}]$ (R = Me, **1** or *i*Pr, **2**). Both structures contain an array of metal centers which describe an approximate "hourglass", with an ammonium cation in the center of each half of the figure. The chromium sites are all six-coordinate, with the two copper sites five-coordinate. The majority of metal–metal edges are bridged by a single fluoride and two pivalate ligands, while two Cr–Cu edges are bridged by a single fluoride and a single pivalate. Magnetic studies show that **1** and **2** exhibit similar (but not identical) behavior, which can be attributed to ten antiferromagnetic and two ferromagnetic exchange interactions around the ring which gives an $S=0$ ground state. Quantum Monte Carlo calculations have been used to quantify the exchange interactions by successfully simulating the susceptibility for the full temperature range and thus clarifying the distinction between **1** and **2**. EPR spectroscopy shows signals due to excited states, and a variable-temperature study has provided an estimate of the energy gap between the first excited state ($S=1$) and second excited state ($S=2$) for **1** that is consistent with the value obtained using the QMC method.

Keywords: ab initio calculations · chromium · cluster compounds · copper · EPR spectroscopy · magnetic properties

Introduction

There are many cyclic polymetallic complexes, ranging as large as the giant wheels made by Müller and co-workers.[1] For 3d metals the most spectacular structure is the $\{Mn_{84}\}$ complex described by the Christou group.[2] There are many other 3d metal rings,[3] dating back to the "ferric wheel"[4] and an octanuclear chromium ring.[5] There are also the many metallocrowns and metallocoronands reported by Pecoraro[6] and Saalfrank's groups.[7] Our interest in such rings began with work on ferromagnetically coupled systems,[8] but more recently has concentrated on heterometallic rings.[9–14] These systems are particularly fascinating because they give the opportunity of studying comparatively simple antiferromagnetically coupled complexes that have a resultant non-zero spin in the magnetic ground state. Such complexes have been proposed as spin Qubits for quantum information processing.[15]

The original heterometallic rings had the general formula $[NH_2R_2][Cr_7MF_8(O_2CCMe_3)_{16}]$ in which R = a linear alkyl chain, for example, Me, Et, or *n*Pr and $M = Ni^{II}$, Co^{II}, Mn^{II}, Fe^{II}. We have shown that using a branched alkyl chain, for example, *i*Pr, leads to a nonanuclear ring[11] with these divalent metal ions. The compounds result as long as M^{II} will adopt an octahedral coordination geometry.

Here we report the chemistry when Cu^{II} is used in a similar reaction, using both Me_2NH and iPr_2NH as templates.

[a] M. Shanmugam, Dr. E. J. L. McInnes, Dr. C. A. Muryn, Dr. G. A. Timco, Prof. R. E. P. Winpenny
School of Chemistry, The University of Manchester
Oxford Road, Manchester, M13 9PL (UK)
Fax: (+44) 161-275-4616
E-mail: richard.winpenny@manchester.ac.uk

[b] L. P. Engelhardt, Prof. Dr. M. Luban
Dept. of Physics & Astronomy, Ames Laboratory
Iowa State University, Iowa, IA 50011 (USA)
Fax: (+1) 515-294-0689
E-mail: luban@ameslab.gov

[c] Prof. F. K. Larsen, J. Overgaard
Department of Chemistry, University of Århus
8000 Århus C (Denmark)

[d] Prof. Dr. E. Rentschler
Institute of Inorganic and Analytical Chemistry
Johannes Gutenberg University of Mainz, Mainz (Germany)

The products have been characterized by X-ray diffraction and studied by magnetic measurements and multifrequency EPR spectroscopy. The results show that while the nuclearity of the complexes are the same, differences are observed in both the variable-temperature susceptibility behavior and the EPR spectra. We have used quantum Monte Carlo (QMC) methods to compute the temperature-dependent susceptibility, and by comparing to experimental data, to determine the magnetic interactions in both compounds.

Results

Synthesis and structural studies: Reaction of hydrated chromium fluoride with pivalic acid and a secondary amine, followed by addition of a source of a divalent 3d metal ion, leads to an octanuclear heterometallic ring if the second metal ion can adopt an octahedral coordination geometry.[8] If basic copper carbonate is used in the same reaction the resulting cage is less easily rationalized [Eq. (1)].

$$10\,CrF_3\cdot 4\,H_2O + 2\,Me_2NH + CuCO_3 \cdot Cu(OH)_2 + 22\,HO_2CCMe_3 \rightarrow [Me_2NH_2]_2[Cr_{10}Cu_2F_{14}(O_2CCMe_3)_{22}]\ (\mathbf{1}) + 16\,HF + 43\,H_2O + CO_2 \quad (1)$$

X-ray diffraction studies (Table 1) of $[Me_2NH_2]_2[Cr_{10}Cu_2F_{14}(O_2CCMe_3)_{22}]$ (**1**) show that a distorted dodecanuclear ring forms in which five Cr^{III} centers lie on both sides of the two Cu^{II} centers (Figure 1). If the same reaction is performed with iPr_2NH a second cyclic dodecanuclear complex is found: $[iPr_2NH_2]_2[Cr_{10}Cu_2F_{14}(O_2CCMe_3)_{22}]$ (**2**; Figure 2). The connectivity within the rings of **1** and **2** is identical; however, the crystallographic symmetry of the two complexes are different. In **1** the molecule lies about an inversion center, while in **2** the entire dodecametallic complex lies within the asymmetric unit.

Table 1. Experimental data for X-ray diffraction studies of **1** and **2**.

	1	**2**
formula	$C_{114}H_{214}Cr_{10}Cu_2F_{14}N_2O_{46}$	$C_{127}H_{242}Cr_{10}Cu_2F_{14}N_2O_{44}$
M_r	3229.95	3414.3
crystal system	tetragonal	monoclinic
space group	$I\,4\,cd$	$P\,2_1/c$
a [Å]	30.950(1)	19.6922(12)
a [Å]		40.8132(19)
c [Å]	37.950(2)	23.8745(120
β [°]	90	101.889(5)
V [Å^3]	36352(3)	18776(2)
T [K]	100(2)	100(2)
Z	8	4
μ [mm^{-1}]	1.178	1.208
unique data	6622	19627
data with $F_o > 4\sigma(F_o)$	5201	13176
$R1/wR2$[a]	0.0977/0.3049	0.1163/0.3081

[a] $R1$ based on observed data, $wR2$ on all unique data.

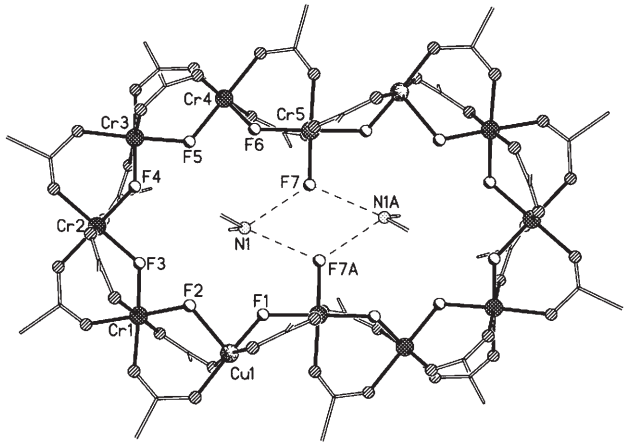

Figure 1. The structure of **1** in the crystal.

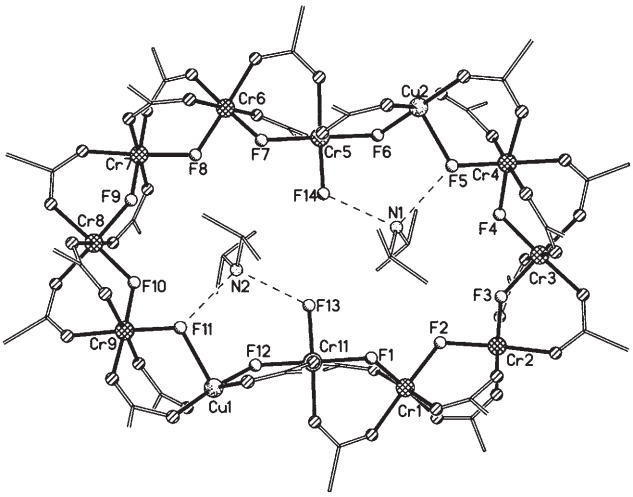

Figure 2. The structure of **2** in the crystal.

For both **1** and **2** the presence of two divalent metal ions makes the ring a dianion. Therefore two secondary ammonium cations are found at the center of the structure and the hydrogen bonding between the cations and the fluorides of the ring differ. In **1** there are hydrogen bonds to the terminal fluorides (N···F 2.65 and 2.77 Å); the next shortest N···F contact is to a fluoride (F1) bridging between Cu1 and the chromium center to which the terminal fluoride is attached (Cr5a) (N···F 3.03 Å). In **2** the hydrogen bonding consists of a two interactions per ammonium, one with a terminal fluoride (N1···F14 2.65, N2···F13 2.67 Å) and the second with an F bridging a Cu^{II} and a Cr^{III} site (N1···F5 2.81, N2···F11 2.77 Å). The next shortest N···F contacts are greater than 3.1 Å and are N1···F6 and N2···F12. It is possibly the need to form hydrogen bonds that leads to a pronounced distortion of the dodecanuclear ring. In previous dodecanuclear rings, the structure is regular, for example, in $\{Ni_{12}\}$[8a] and $\{Co_{12}\}$ rings[8b] the molecule has S_6 crystallographic symmetry, while in a recently reported $\{Fe_{12}\}$ ring[16] the array of metal centres has approximate sixfold symmetry.

All the Cr^{III} sites in **1** and **2** are six-coordinate. In both structures eight chromium centers have four O and two F atoms in their coordination spheres, which is typical for heterometallic rings.[9–12,14] The final two Cr sites, which are symmetry-related in **1** (Cr5 and Cr5a) but not in **2** (Cr5 and Cr11) are bound to three O and three F donors; the additional fluorides attached to these ions are the only terminal ligands in the structure, and point into the cavity within the metallomacrocycle. Bond lengths and angles are listed in Table 2 and are typical for chromium.

Table 2. Selected bond length [Å] and angle [°] ranges for **1** and **2**.

	1	**2**[a]
Cu–F(ap)	2.103(9)	2.183(7)–2.212(7)
Cu–F(eq)	1.886(10)	1.890(9)–1.917(7)
Cu–O	1.919(14)–1.962(12)	1.877(17)–1.929(11)
Cr–F(bridge)	1.885(9)–1.931(10)	1.866(7)–1.941(8)
Cr–F(terminal)	1.847(10)	1.861(7)–1.866(7)
Cr–O	1.896(15)–2.009(14)	1.896(12)–1.989(12)
F(ap)-Cu-O	91.7(5)–98.1(5)	89.6(8)–99.3(9)
cis F(eq)-Cu-O	90.1(5)–92.8(5)	87.0(6)–95.2(4)
trans F(eq)-Cu-O	177.2(5)	172.2(9)*–174.6(4)
F(ap)-Cu-F(eq)	84.6(4)	89.6(3)–92.3(3)
cis O-Cu-O	88.2(6)–88.6(6)	85.9(5)–91.8(5)
trans O-Cu-O	170.0(6)	163.2(6)–165.3(5)
cis F-Cr-F	87.3(4)–91.0(5)	88.7(3)–91.6(3)
trans F-Cr-F	178.5(5)	179.1(3)–179.2(3)
cis F-Cr-O	86.6(5)–95.5(5)	87.4(4)–93.3(3)
trans F-Cr-O	176.2(5)–179.7(9)	176.0(5)–178.6(4)
cis O-Cr-O	85.3(6)–95.3(6)	84.5(5)–92.9(5)
trans O-Cr-O	175.3(5)–179.1(9)	175.4(4)–178.5(4)

[a] Bond lengths and angles involving disordered pivalates excluded except for angle identified with *.

The copper sites are all five-coordinate, with a square-based pyramidal geometry; three O and one F donors are bound in the basal plane, with a fluoride ligand in the axial position. The Cu–O bond lengths fall in the range 1.877(17)–1.962(12) Å. The bonds to the basal fluorides vary from 1.886(1) to 1.917(7) Å, with the bond to the apical F-site longer in all cases and falling in the range 2.103(9)–2.212(7) Å.

As bond angles at single-atom bridges can be related to the magnitude of the magnetic superexchange, it is worth considering the angles at the bridging fluorides **1** and **2**. In **1** the eight Cr-F-Cr angles range from 123.0(5)–125.0(6)°, averaging 124.0°. In **2** the eight equivalent angles range from 123.7(3)–125.3(3)°, with an average of 124.9°. The Cr-F-Cu angles fall into two groups. Firstly there are those involving the F ligand in the Cu basal plane. In **1** this angle is 122.5(5)°, while in **2** this angle is much bigger, averaging 130.9(5)±1.1°; such a significant difference could influence the magnitude of the magnetic exchange, especially as the magnetic orbital of Cu^{II} ($d_{x^2-y^2}$) should interact with this fluoride. The bridging angle involving the apical fluoride is similar for the two compounds: 113.0(5)° in **1** and 114.5(3) and 114.7(3)° in **2**. Whether this fluoride influences the magnetic exchange is debatable as it does not interact with the SOMO on Cu^{II}. The prediction, based on this structural evidence, and the assumption that superexchange through fluoride is the most important path for magnetic interactions, is that the only significant difference we should observe would be in the magnitude of one exchange interaction between Cr and Cu.

A final point concerning the two structures is the degree of disorder found. While pivalate ligands are very frequently disordered, due to disorder of the *tert*-butyl groups of the carboxylate, in **2** there is additional disorder in which one of the two carboxylates bridging Cu2 and Cr4 adopts two distinct conformations, including the O atoms bound to the metal centers. These metal centers therefore have a disordered coordination sphere. This may be important in explaining why the EPR spectra of **2** are a great deal less well resolved than those of **1** (see below); disorder can introduce strain in both the *g* and *D* tensors.

Magnetic measurements: For both **1** and **2** the product $\chi_m T$ has a value of about 16 $cm^3 K mol^{-1}$ at room temperature (Figure 3). This compares with a calculated value of

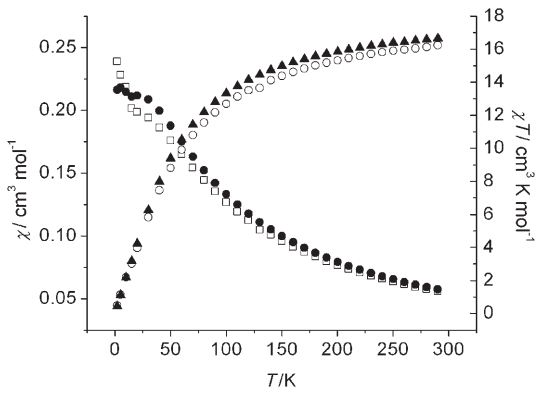

Figure 3. The variable temperature behavior of **1** and **2** displayed as: χ_m versus *T*, □ for **1** and ● for **2**; and $\chi_m T$ versus *T*, ○ for **1** and ▲ for **2**. The measurements were made in a 1 T magnetic field.

19.4 $cm^3 K mol^{-1}$ for ten noninteracting Cr^{III} and two noninteracting Cu^{II} centers (assuming $g_{Cr}=1.99$, $g_{Cu}=2.1$). The measured value of $\chi_m T$ declines steadily as temperature falls, and at the lowest temperature measured (1.8 K) in both cases is less than 1 $cm^3 K mol^{-1}$, suggesting predominantly antiferromagnetic exchange and a likely $S=0$ ground state. This is entirely predictable given that the Cr···Cr exchange is antiferromagnetic in all the heterometallic rings we have studied.

The behavior of χ_m shows a subtle difference between **1** and **2** below 50 K. For **1** the increase in χ_m with decreasing *T* slows, and a small plateau begins to form, but below 15 K the value increases sharply. This behavior would be consistent with an $S=0$ ground state only if χ_m falls towards zero below the lowest measured temperature (1.8 K). The value of χ_m for **2** is slightly larger than that for **1** for $T>10$ K, and a noticeable plateau forms for lower temperatures. There is a second maxima—with the value of χ_m at 2 K slightly higher than at 4 K.

EPR spectroscopy: While the differences in the susceptibility behavior of **1** and **2** are subtle, the differences in the EPR spectra of the two compounds are more pronounced. Studies of **1** at K- or Q-band show a broad unresolved resonance at 20 K and above. This is typical for exchange-coupled compounds when several spin multiplets are occupied. However, at 10 K and below the spectrum is resolved into a series of features (Figure 4). At the Q-band, we find a strong feature

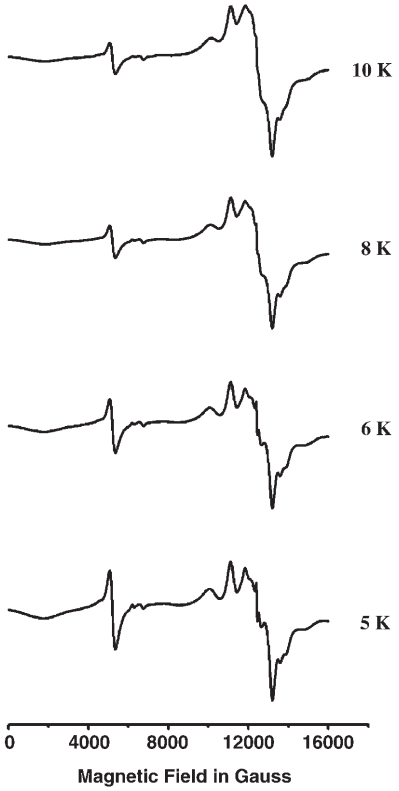

Figure 4. Variable temperature EPR spectra of **1** recorded at Q-band (34 GHz).

at $B=5000$ G, a complex series of lines centered at $B=13000$ G, and many weaker resonances. The low-field feature resembles the $\Delta m_s=2$ transition of an $S=1$ state, and the different temperature-dependent behavior of the various resonances suggests that we are seeing more than one spin state. The feature at low field increases in intensity relative to the rest of the spectrum as temperature falls, suggesting that it arises from a spin state lower in energy than the spin state responsible for the lines near $B=13000$ G. The spectra of **2** show different behavior (Figure 5). At 20 K and above there is a broad unresolved signal centered at $g=2.00$. At lower temperatures structure appears on this resonance, but even at 5 K this structure is not resolved.

Discussion

Possible spin ground states of a {$Cr_{10}Cu_2$} cycle: Prior to a discussion of the quantitative analysis of the magnetism, it is useful to first consider the possible spin ground states resulting from classical considerations. In fact, these considerations will clarify the inadequacy of the method used in our previous paper on this system. In that paper we used a hypothetical {Cr_8Cu_2} ring as a model. This followed a similar procedure to that adopted for {Fe_{10}} rings previously.[4] Unfortunately while this substitution is valid in a homometallic ring, the nuclearity of the heterometallic ring makes this approach invalid as will be explained in the following with the aid of Figure 6.

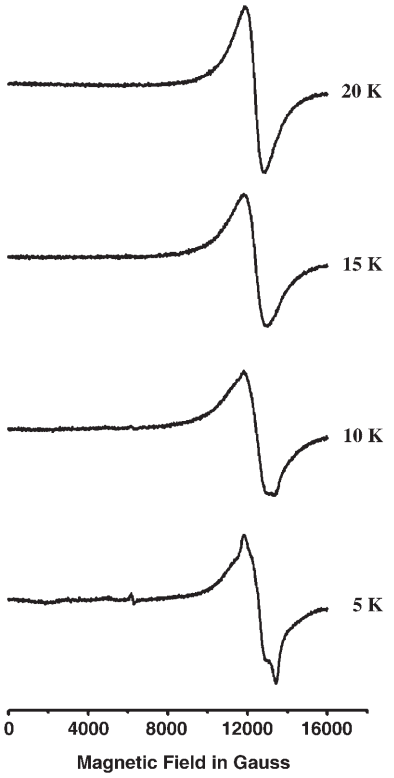

Figure 5. Variable temperature EPR spectra of **2** recorded at Q-band (34 GHz).

We consider two possible sets of exchange parameters. Firstly, in model **A** all exchange parameters around the {$Cr_{10}Cu_2$} cycle are antiferromagnetic (Figure 6, model **A**). If we number the metal sites sequentially from 1 to 12, the two Cu^{II} ions are found in positions 1 and 7 of the cycle. Therefore if we consider the magnetic behavior of sublattices of the ring containing the metal ions in the "odd" positions we would get the spin from the odd sublattice as:

$$S_{odd}=4\times3/2\ (\text{from } Cr^{III}) + 2\times1/2\ (\text{from } Cu^{II})=7.$$

For the even sublattice the spin would be given by:

$$S_{even}=6\times\text{-}3/2\ (\text{all from } Cr^{III})=-9.$$

The ground state would therefore have $S=2$ from coupling the odd sites antiferromagnetically to the even.

If we assume that two of the four Cr···Cu exchange interactions are ferromagnetic this generates model **B**, which can

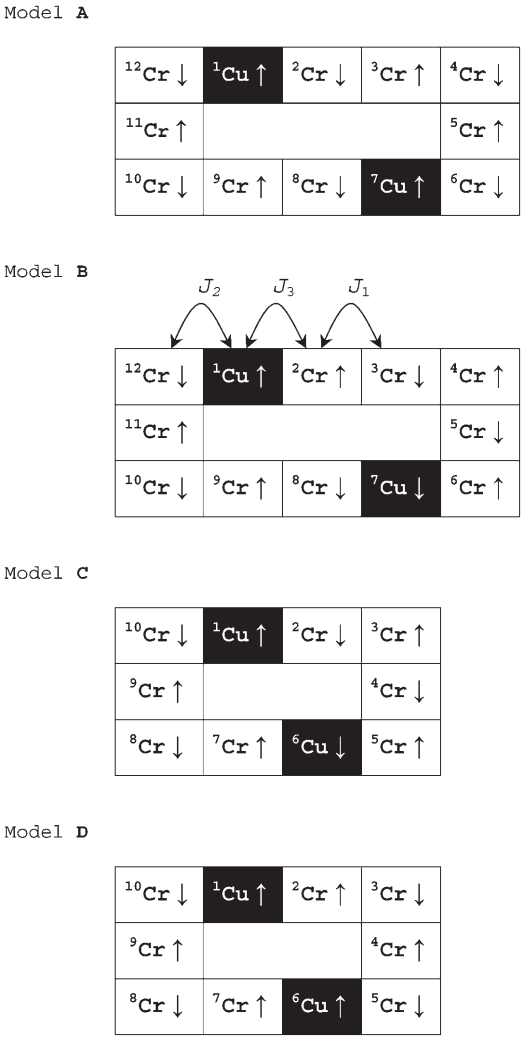

Figure 6. Schematic representation of possible ground states for cyclic $\{Cr_{10}Cu_2\}$ and $\{Cr_8Cu_2\}$ compounds.

be shown to have an $S=0$ ground state (Figure 6). Thus the presence of two ferromagnetic exchange interactions generates a lower spin ground state than all antiferromagnetic interactions.

Unfortunately when an imaginary $\{Cr_8Cu_2\}$ ring is considered, as in our previous paper, the result is almost the opposite. The two Cu^{II} sites are at 1 and 6 within the decametallic cycle, and hence one belongs to each of the odd and even sublattices. Therefore for model **C**, in which all nearest neighbor interactions are antiferromagnetic, the spin ground state is 0. Introduction of two ferromagnetic interactions gives model **D**, which would have an $S=1$ ground state.

Therefore while for $\{Cr_{10}Cu_2\}$ inclusion of two F-exchange interactions gives an $S=0$ ground state (model **B**), for the imaginary $\{Cr_8Cu_2\}$ ring the diamagnetic state arises from the all antiferromagnetic model **C**.

Quantum Monte Carlo simulations: Detailed analysis of the magnetism by using full-matrix diagonalisation would be impractical because a cyclic $\{Cr_{10}Cu_2\}$ array involves matrices of 4.2×10^6 rows and columns. Instead we used the QMC method to derive the exchange constants. Our earlier analysis of the bond angles suggested that we adopt a model based on three exchange constants J_1, J_2, and J_3. Additionally, the qualitative analysis of the previous subsection, based on a classical picture of the spins, as shown in Figure 6 (model **B**), suggests an expected $S=0$ ground state. Using a quantum Monte Carlo (QMC) method to calculate χ_m versus T, we were able to provide a quantitative foundation for this model. Our analysis allowed us to 1) improve upon the previously published estimates of J_1, J_2, J_3, 2) establish the spin of the ground state, and 3) clarify the distinction between the two compounds based on the susceptibility data. The indispensable advantage of this method is that the susceptibility is calculated in a manner that is free from systematic errors, while avoiding the severe obstacles of diagonalizing very large matrices.

We use the Hamiltonian given in Equation (2) in which $\vec{s}_{13}\equiv\vec{s}_1$, and the $J(n)$ are set equal to J_1 for Cr–Cr pairs and either J_2 or J_3 for Cr–Cu pairs (see Figure 6).

$$H=\sum_{n=1}^{12}\left[J(n)\vec{s}_n\cdot\vec{s}_{n+1}+g(n)\mu_B\vec{s}_n\cdot\vec{B}\right] \quad (2)$$

Also, $g(n)$ is chosen equal to 1.96 for Cr ions and 2.1 for Cu ions. We calculated χ_m versus T for a very large number of (J_1, J_2, J_3) triplets. From the data it was immediately evident that, for temperatures above 100 K, χ_m is relatively insensitive to J_2 and J_3. Thus, by fitting the high-temperature data, we were able to determine the value of the antiferromagnetic Cr–Cr exchange and found that for **1** $J_1=-20\pm0.5$ K and for **2** $J_1=-17.5\pm0.5$ K.

Although the high-temperature susceptibility is determined almost entirely by J_1, we found that the low-temperature data is extremely sensitive to even slight variations in the two Cr-Cu exchange interactions, J_2 and J_3. This can be seen in the contour maps of Figure 7, in which we show that by varying J_2 or J_3 by only a few K the resulting fits to the experimental data become orders of magnitude worse. Also demonstrated by this figure, there is only a single, small region in the three dimensional (J_1, J_2, J_3) parameter space that produces a good fit. For **1**, this best fit is achieved with the values $J_2=-22\pm1$ K and $J_3=+13\pm1$ K, while for **2** we find $J_2=-26\pm1$ K and $J_3=+18\pm1$ K.

In Figure 8 we present the experimental susceptibility for **1** and **2** as well as the QMC data that yield the best fits. Note that in both cases the fits are very good. We successfully reproduce the plateau and the rapid increase at lower temperatures for **1**, as well as the "double maxima" below 50 K for **2**. The QMC calculations are easily extended to lower temperatures, and for both sets of exchange parameters, we find that the theoretical data drops towards zero below 1 K. This indicates that the spin ground state is indeed zero.

Based on the exchange parameters given above, additional QMC calculations were performed so as to obtain M

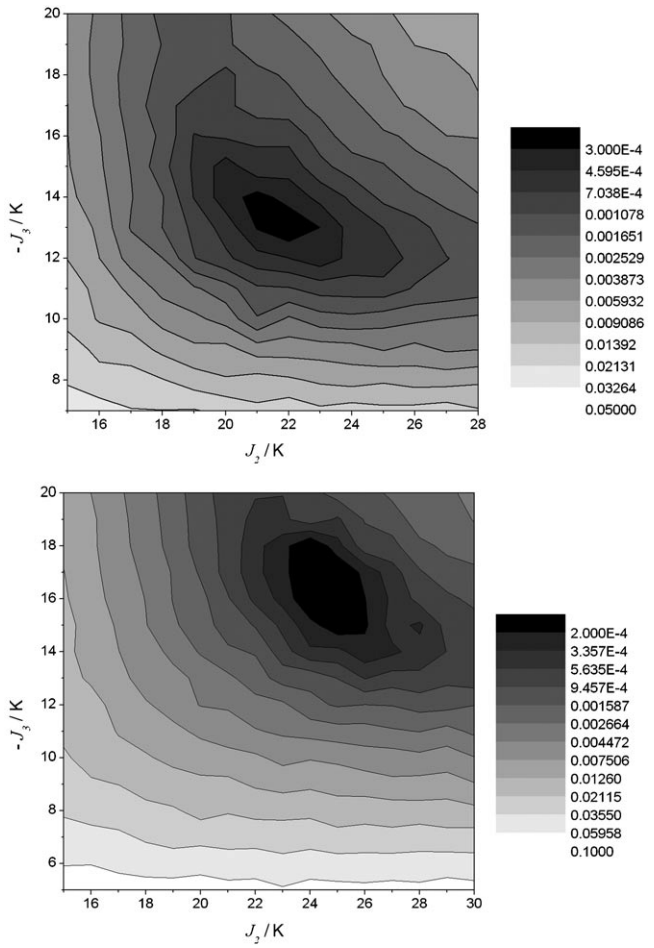

Figure 7. Contour maps showing variation of quality of fit of data with variation of J_2 and J_3 for the fixed choices $J_1 = -20$ K for **1** (top) and $J_2 = -17.5$ for **2** (bottom). The gray scale bars summarize the discrepancy between the experimental and QMC $\chi(T)$ data for **1** (top) and **2** (bottom).

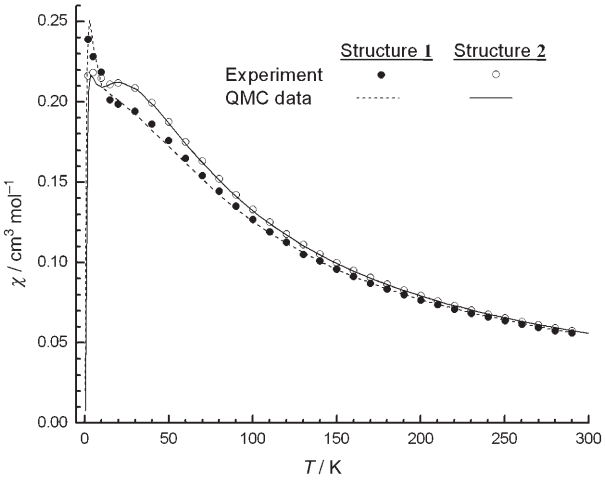

Figure 8. QMC fit of susceptibility behavior of **1** and **2** using the parameters given in the text.

versus B for several very low temperatures. Analysis of this data allows us to predict the energy gaps between the $S=0$ ground state and the lowest $S=1$ and $S=2$ states. Based on these calculations, for **1** the S = 1 state lies 2.0 cm^{-1} above the ground state and the $S=2$ state is 6.5 cm^{-1} above the ground state. For **2** the $S=1$ state is 2.3 cm^{-1} and the $S=2$ state is 7.5 cm^{-1} above the ground state.

The beauty of the QMC method is that it allows us to quickly survey all possible variations of the exchange interactions. In a few hours of computation using five nodes of a computer cluster, we were able to consider hundreds of different choices of the three exchange constants, while the corresponding calculations using diagonalization methods would take several years. It is particularly intriguing that features which might otherwise be attributed to "impurities", such as the rapid increase in **1** at low temperatures, can be reproduced by a model without any impurities. Moreover, it is satisfying that we can differentiate between **1** and **2** by different sets of exchange constants although they have very similar sets of data.

Analysis of the EPR spectroscopic data: The differences between the spectra of **1** and **2** are significant, and we will propose explanations for these differences below.

The spectra of **1** show the presence of at least two spin states. We initially thought that, if the ground state is $S=0$, these states would be the $S=1$ first excited state and the $S=2$ second excited state. We have therefore simulated the spectra by adding together the spectra due to both spin triplet (Figure 9 $S=1$) and spin quintet states (Figure 9 $S=2$).

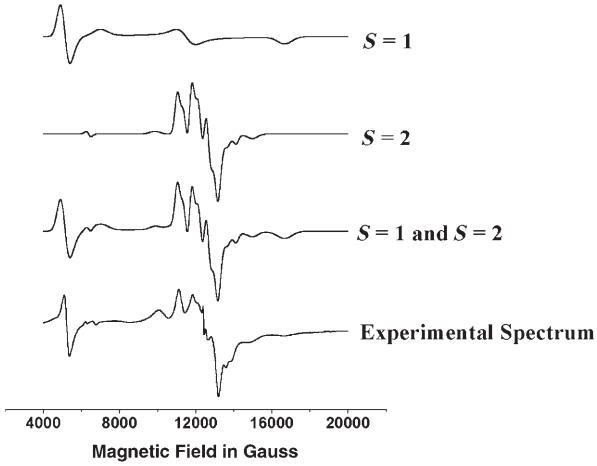

Figure 9. Analysis of the EPR spectrum of **1**. Simulations of the $S=1$ and S = 2 states and the sum of the $S=1$ and 2 states; experimental EPR spectra for **1** at 5 K and Q-band is also given. The simulations use the parameters given in the text.

We can achieve the simulation shown in Figure 9 by using the following parameters: for $S=1$, $g_x = g_y = g_z = 2.03$, $D_{S=1} = 0.455$ cm^{-1}, $\lambda = 0.33$, $W_x = W_y = W_z = 450$ G; for $S=2$, $g_x = 1.97$, $g_y = 1.90$, $g_z = 1.95$, $D_{S=2} = 0.078$ cm^{-1}, $\lambda = 0$, $W_x = W_y = 145$ G, $W_z = 300$ G, in which W_i are Gaussian linewidths.

The observation of spectra for two spin states also allows us to pursue a more involved analysis. The first idea was to derive the single-ion contribution to the cluster spin Hamil-

tonian parameters by using the spin projection approach.[17] As Cu^{II} is an $S=1/2$ ion it has $D=0$. The spin projection approach involves pair-wise coupling of spins, using Equation (3),[17] in which d_1, d_2, and d_{12} are coefficients straightforwardly calculated from the coupled spin states, D_A and D_B are the single-ion axial zero-field splitting parameters for spin A and spin B, respectively, and D_{AB} is the exchange contribution to the zero-field splitting of the specific spin state of the cluster, D_s.

$$D_s = d_1 D_A + d_2 D_B + d_{12} D_{AB} \tag{3}$$

The difficulty in applying this method to such a complex system is that we have to define a coupling scheme for the order in which we couple the spins of the cluster.[18,19]

The one we have chosen is to consider the cyclic cluster to contain two identical sublattices that couple antiferromagnetically to give the spin ground state. Each sublattice contains a *ferromagnetically* coupled nearest neighbor Cr–Cu pair, giving an $S=2$ state, and two *ferromagnetically* aligned pairs of Cr^{III} ions that are next-nearest neighbors, each giving an $S=3$ state. To generate the $S=8$ for the sublattice we couple firstly the Cr ions in each pair and then couple these pairs to give an $S=6$ state; we then coupled this $S=6$ state to the $S=2$ from the Cr–Cu pair to give $S=8$. The same procedure was followed for the second sublattice and in the final step these two $S=8$ states were coupled to generate the $S=1$ and $S=2$ states observed (as well as all other states from $S=0$ to $S=16$). Using this approach we can calculate how $D_{S=1}$ and $D_{S=2}$ depend on D_{Cr} and on a series of exchange terms [Eqs. (4) and (5)]

$$D_{S=1} = \frac{-57}{8} D_{Cr} - 57\left(\frac{3}{40} D_{CrCr} + \frac{1}{80} D_{CrCu} + \frac{3}{20} D_{3.3} + \frac{1}{5} D_{6.2}\right) + 29 D_{8.8} \tag{4}$$

$$D_{S=2} = \frac{-13}{8} D_{Cr} - 13\left(\frac{3}{40} D_{CrCr} + \frac{1}{80} D_{CrCu} + \frac{3}{20} D_{3.3} + \frac{1}{5} D_{6.2}\right) + 7 D_{8.8} \tag{5}$$

The various exchange terms are labeled as either the ions involved in the exchange (D_{CrCr} or D_{CrCu}) or the intermediate spin states involved ($D_{3,3}$ or $D_{6.2}$ or $D_{8.8}$). Unfortunately this generates two simultaneous equations in six unknowns. We can easily eliminate five of the unknowns by multiplying one equation by 13 and the other by 57 then subtracting, leaving an equation in $D_{8.8}$ [Eq. (6)]

$$57 D_{S=2} - 13 D_{S=1} = 22 D_{8.8} \tag{6}$$

Including the measured values for $D_{S=2}$ and $D_{S=1}$ gives $D_{8.8} = -0.07\ cm^{-1}$. If we include this value in the equations for $D_{S=2}$ and $D_{S=1}$ and neglect the other exchange terms we get Equations (7).

$$D_{S=1} = \frac{-57}{8} D_{Cr} - 1.94$$
$$D_{S=2} = \frac{-13}{8} D_{Cr} - 0.47 \tag{7}$$

This gives $D_{Cr} = 0.34\ cm^{-1}$, which is very similar to the single-ion contributions to anisotropy determined in other heterometallic rings by inelastic neutron scattering.[20] The procedure is reasonable as, assuming dipolar exchange as the largest contributor to the exchange term, the $D_{8.8}$ term should be the largest as it involves the largest two intermediate spins; it also has the largest coefficient in the equations.

The second piece of analysis uses the different variable temperature behavior of the resonances due to the $S=1$ and $S=2$ spin states to attempt to derive the energy gap between these states. The analysis uses the fact that the intensity of an EPR transition is proportional to the contribution to the magnetic susceptibility of a specific state. Using the Van Vleck equation, and assuming that at low temperature only the $S=0$, 1, and 2 states are populated, we can calculate the contributions to the total susceptibility from the $S=1$ and $S=2$ states and set them as proportional to intensities. This gives Equations (8) and (9) in which $I_{S=1}$ and $I_{S=2}$ are the intensities of the signals due to the relevant spin states, E_1 is the energy of the $S=1$ state and E_2 is the energy of the $S=2$ state (setting the energy of the $S=0$ ground state as zero).

$$I_{S=1} \propto \frac{\left(2N\frac{g^2\beta^2}{kT}\right)\left(\exp\left(-\frac{E_1}{kT}\right)\right)}{1 + 3\exp\left(-\frac{E_1}{kT}\right) + 5\exp\left(-\frac{E_2}{kT}\right)} \tag{8}$$

$$I_{S=2} \propto \frac{\left(10N\frac{g^2\beta^2}{kT}\right)\left(\exp\left(-\frac{E_2}{kT}\right)\right)}{1 + 3\exp\left(-\frac{E_1}{kT}\right) + 5\exp\left(-\frac{E_2}{kT}\right)} \tag{9}$$

If we assume the same proportionality constant and divide one equation by the other and convert to a logarithmic scale we get Equation (10).

$$\ln I_{S=1} - \ln I_{S=2} = (E_2 - E_1/kT) - \ln(5) \tag{10}$$

Therefore a plot of the difference in the logs of the intensities versus $1/T$ will give the energy gap as the slope. Comparing the intensities of the two spin states was done by identifying specific isolated resonances that could be assigned exclusively to either the $S=1$ or $S=2$ states and considering the relative amplitudes of these resonances. In all cases the energy gap is found to be between 4.8 and $6.0\ cm^{-1}$. Due to the difficulty in accurately measuring intensities of EPR lines, we are satisfied that this estimate is consistent with the result, $4.5\ cm^{-1}$, that we obtained for **1** using the QMC method (see above).

The unresolved question concerning the EPR spectra is the considerable difference between the spectra of **2** and **1**. The best explanation we can propose is that the disorder in the coordination sphere of two metal centers in **2** (Cu2 and Cr4, see above) introduces strain into both the *g* and *D* tensors. This causes the $S=1$ state to give resonances that are broadened beyond being noticeable (we can see some very broad peaks in the baseline at low field), while the $S=2$ state gives a much less well resolved set of lines than for **1**. Other possible explanations, for example, very large zero-field splitting of the $S=1$ state that would take the resonances out of the spectral window, do not seem plausible. The explanation that the $S=2$ state is lowest in energy (model **A** in Figure 6) cannot be reconciled with the magnetic data.

Conclusion

The results presented here show how the coordination geometry of the divalent metal influences the structure of heterometallic rings, in which the divalent metal adopts an octahedral coordination geometry regular octagonal rings are formed from the reaction described here.[9] The resolution of the EPR spectra of **1** has allowed us to derive both the single-ion anisotropy of the Cr^{III} ions present and the energy gap between the $S=1$ and $S=2$ states.

The most intriguing results come from the magnetic analysis using QMC methods. The speed of the method allows us to survey parameter space very quickly and this has allowed us to fit the data without invoking a paramagnetic impurity to explain a low temperature rise in χ_m. The time constraints created by the slowness of traditional diagonalisation methods prevents a full survey of parameter space; it is possible that in previous work this has led workers to include a "paramagnetic impurity" as a short-cut to fitting data well even though no impurity was present.

Experimental Section

Preparation of compounds: All reagents, metal salts and ligands were used as obtained from Aldrich. Analytical data were obtained by the microanalytical service of the University of Manchester.

Compound 1: $CrF_3{\cdot}4H_2O$ (3.0 g, 17 mmol), dimethylamine (3.0 mL, 2.0 M solution in tetrahydrofuran, 6.0 mmol), and pivalic acid (14.0 g, 140 mmol) were stirred together at 140 °C for 2.0 h in a Teflon flask. Basic copper carbonate (1.0 g, 4.5 mmol) was added and the solution heated for a further 3 h. The flask was cooled to room temperature and acetone (30 mL) was added with stirring. A green crystalline product was formed. The product was filtered, washed with a large quantity of acetone, dried in air and recrystallized from ethylacetate:acetone (1:1). Yield 3.2 g (60%); elemental analysis calcd (%) for $C_{114}H_{214}Cr_{10}Cu_2F_{14}N_2O_{44}{\cdot}2\,EtOAc$: Cr 15.27, Cu 3.73, C 43.02, H 6.81, N 0.82, F 7.81; found: Cr 14.93, Cu 3.76, C 43.47, H 7.04, N 0.68, F 7.23.

Compound 2: $CrF_3{\cdot}4H_2O$ (5.0 g, 27.6 mmol), diisopropylamine, (1.2 g, 11.9 mmol), basic copper carbonate (0.55 g, 2.5 mmol) and pivalic acid (15.0 g, 147 mmol) were heated while stirring at 140 °C for 6.0 h. The flask was cooled to room temperature and acetone (30 mL) was added; the obtained solution was filtered and then diluted with acetonitrile (30 mL) causing precipitation of the green product. This was collected, washed with acetonitrile, and dried in air, followed by purification by column chromatography on silica gel using ethyl acetate as eluent; **2** was eluted as the first product. The eluent was evaporated to dry under reduced pressure. The product was crystallized from a pentane/acetone mixture by slow evaporation of the solvents. Yield 1.75 g (21%, calculated from Cu); elemental analysis calcd(%) for $C_{122}H_{230}Cr_{10}F_{14}N_2Cu_2O_{44}$: Cr 15.56, Cu 3.80, C 43.84, H 6.94, N 0.84, F 7.96; found: Cr 15.99, Cu 3.64, C 43.74, H 7.20, N 0.75, F 7.87.

X-ray diffraction studies: Data were collected on Bruker SMART CCD diffractometer ($Mo_{K\alpha}$, $\lambda=0.71069$ Å). In all cases the selected crystals were mounted on the tip of a glass pin using Paratone-N oil and placed in the cold flow (120 K) produced with an Oxford Cryocooling device. Complete hemispheres of data were collected using ω-scans (0.3°, 30 seconds/frame). Integrated intensities were obtained with SAINT+[21] and they were corrected for absorption using SADABS.[21] Structure solution and refinement was performed with the SHELX package.[21] The structures were solved by direct methods and completed by iterative cycles of ΔF syntheses and full-matrix least-squares refinement against F^2.

CCDC-610559 and 610560 contain the supplementary crystallographic data for this paper. These data can be obtained free of charge from the Cambridge Crystallographic Data Centre via www.ccdc.cam.ac.uk/data_request/cif.

Acknowledgements

This work was supported by the EPSRC (UK), including the UK National Computing Service, and INTAS Grant No 03-51-4532. We are also very grateful to Dr David Collison for helpful discussions. The Ames Laboratory is operated for the United States Department of Energy by Iowa State University under contract No. W-7405-Eng-82.

[1] A. Müller, E. Krickemeyer, J. Meyer, H. Bögge, F. Peters, W. Plass, E. Diemann, S. Dillinger, F. Nonnebruch, M. Randerath, C. Menke, *Angew. Chem.* **1995**, *107*, 2293–2295; *Angew. Chem. Int. Ed. Engl.* **1995**, *34*, 2122–2124.

[2] A. Tasiopoulos, A. Vinslava, W. Wernsdorfer, K. A. Abboud, G. Christou, *Angew. Chem.* **2004**, *116*, 2169–2173; *Angew. Chem. Int. Ed.* **2004**, *43*, 2117–2121; .

[3] R. E. P. Winpenny, *Compr. Coord. Chem. II* **2004**, *7*, 125–175, and references therein.

[4] K. L. Taft, C. D. Delfs, G. C. Papaefthymiou, S. Foner, D. Gatteschi, S. J. Lippard, *J. Am. Chem. Soc.* **1994**, *116*, 823.

[5] N. V. Gerbeleu, Yu. T. Struchkov, G. A. Timco, A. S. Batsanov, K. M. Indrichan, G. A. Popovich, *Dokl. Akad. Nauk SSSR* **1990**, *313*, 1459–1462.

[6] V. L. Pecoraro, A. J. Stemmler, . B. R. Gibney, J. J. Bodwin, H. Wang, J. W. Kampf, A. Barwinski, *Prog. Inorg. Chem.* **1997**, *45*, 83–117.

[7] for example, O. Waldmann, R. Koch, S. Schromm, J. Schülein, P. Müller, I. Bernt, R. W. Saalfrank, F. Hampel, E. Balthes, *Inorg. Chem.* **2001**, *40*, 2986–2995 and refs therein.

[8] a) H. Andres, R. Basler, A. J. Blake, E. K. Brechin, C. Cadiou, G. Chaboussant, C. M. Grant, H.-U. Güdel, S. G. Harris, M. Murrie, S. Parsons, C. Paulsen, F. Semadini, V. Villar, W. Wernsdorfer, R. E. P. Winpenny, *Chem. Eur. J.* **2002**, *8*, 4867–4876; b) E. J. L. McInnes, C. Anson, A. K. Powell, A. J. Thomson, S. Poussereau, R. Sessoli, *Chem. Commun.* **2001**, 85–86; c) E. K. Brechin, O. Cador, A. Caneschi, C. Cadiou, S. G. Harris, S. Parsons, M. Vonci, R. E. P. Winpenny, *Chem. Commun.* **2002**, 1860–1861.

[9] F. K. Larsen, E. J. L. McInnes, H. El Mkami, J. Overgaard, S. Piligkos, G. Rajaraman, E. Rentschler, A. A. Smith, G. M. Smith, V. Boote, M. Jennings, G. A. Timco, R. E. P. Winpenny, *Angew. Chem.* **2003**, *115*, 105–109; *Angew. Chem. Int. Ed.* **2003**, *42*, 101–105.

[10] F. K. Larsen, J. Overgaard, S. Parsons, E. Rentschler, G. A. Timco, A. A. Smith, R. E. P. Winpenny, *Angew. Chem.* **2003**, *115*, 6160–6163; *Angew. Chem. Int. Ed.* **2003**, *42*, 5978–5981.
[11] O. Cador, D. Gatteschi, R. Sessoli, F. K. Larsen, J. Overgaard, A.-L. Barra, S. J. Teat, G. A. Timco, R. E. P. Winpenny, *Angew. Chem.* **2004**, *116*, 5308–5312; *Angew. Chem. Int. Ed.* **2004**, *43*, 5196–5200.
[12] S. L. Heath, R. H. Laye, C. A. Muryn, R. Sessoli, R. Shaw, S. J. Teat, G. A. Timco, R. E. P. Winpenny, *Angew. Chem.* **2004**, *116*, 6258–6261; *Angew. Chem. Int. Ed.* **2004**, *43*, 6132–6135.
[13] R. H. Laye, F. K. Larsen, J. Overgaard, C. A. Muryn, E. J. L. McInnes, E. Rentschler, V. Sanchez, H. U. Güdel, O. Waldmann, G. A. Timco, R. E. P. Winpenny, *Chem. Commun.* **2005**, 1125–1127.
[14] G. A. Timco, A. S. Batsanov, F. K. Larsen, C. A. Muryn, J. Overgaard, S. J. Teat, R. E. P. Winpenny, *Chem. Commun.* **2005**, 3649–3651.
[15] F. Troiani, A. Ghirri, M. Affronte, S. Carretta, P. Santini, G. Amoretti, S. Piligkos, G. A. Timco, R. E. P. Winpenny, *Phys. Rev. Lett.* **2005**, *94*, 207208–207211.
[16] C. P. Raptopoulou, V. Tangoulis, E. Devlin, *Angew. Chem.* **2002**, *114*, 2492–2495; *Angew. Chem. Int. Ed.* **2002**, *41*, 2386–2389.
[17] A. Bencini, D. Gatteschi, *EPR of Exchange Coupled Systems*, Springer, Berlin **1989**.
[18] A-L. Barra, D. Gatteschi, R. Sessoli, *Phys. Rev. B* **1997**, *56*, 8192.
[19] D. Collison, M. Murrie, V. S. Oganesyan, S. Piligkos, N. R. J. Poolton, G. Rajaraman, G. M. Smith, A. J. Thomson, G. A. Timco, W. Wernsdorfer, R. E. P. Winpenny, E. J. L. McInnes, *Inorg. Chem.* **2003**, *42*, 5293–5303.
[20] R. Caciuffo, T. Guidi, S. Carretta, P. Santini, G. Amoretti, C. Mondelli, G. A. Timco, R. E. P. Winpenny, *Phys. Rev. B* **2005**, *71*, 174407/1–174407/8.
[21] SHELX-PC Package, Bruker Analytical X-ray Systems, Madison, WI, **1998**.

Received: June 13, 2006
Published online: September 29, 2006

